Enhanced intrinsic photocatalytic activity of TiO$_2$ electrospun nanofibers based on temperature assisted manipulation of crystal phase ratios

Ammara Riaz
State Key Laboratory of Silicon Materials, School of Materials Science and Engineering, Zhejiang University, Hangzhou 310027, People's Republic of China

Hejinyan Qi and Yuan Fang
School of Materials Science and Engineering, Tianjin University, Tianjin 300072, People's Republic of China

Jianfeng Xu and Chunmei Zhou[a)]
State Key Laboratory of Silicon Materials, School of Materials Science and Engineering, Zhejiang University, Hangzhou 310027, People's Republic of China

Zhengguo Jin
School of Materials Science and Engineering, Tianjin University, Tianjin 300072, People's Republic of China

Zhanglian Hong, Mingjia Zhi, and Yi Liu
State Key Laboratory of Silicon Materials, School of Materials Science and Engineering, Zhejiang University, Hangzhou 310027, People's Republic of China

TiO$_2$ nanofibers (TNFs) with different anatase/rutile phase ratios were fabricated using electrospinning technique followed by the annealing at different temperatures. The effect of annealing temperatures on their morphology, structural, and optical properties and photocatalytic activity was investigated. The photocatalytic performance of TNFs was evaluated by degradation of methyl orange (MO) in aqueous solution under the irradiation of simulated solar light. Annealing temperature significantly influenced photocatalytic degradation of MO due to the incorporation of rutile phase which suppresses recombination of photoactivated electron and hole pairs. Turnover frequency (TOF) of MO degradation was introduced to describe the intrinsic activity of TNFs. TNFs acquired best anatase/rutile phase ratio (A/R = 83/17) when annealed at 650 °C, resulting in highest TOF value 2394 h^{-1}, two times higher as compared to P25 with similar anatase/rutile phase ratio (A/R = 85/15). Appropriate crystalline structure could be the reason for good photocatalytic activity as well as intrinsic activity of TNFs.

I. INTRODUCTION

The beginning of TiO$_2$ photocatalysis was in the early seventies when Honda and Fujishima reported the decomposition of water to hydrogen on the surface of TiO$_2$ electrodes under light irradiation.[1] Recently, a combined effect of growing population and a rapidly developing industry has resulted in a steady increase of water pollution in many parts of the world due to the accelerated release of harmful agents.[2] During past few decades, photocatalysis has emerged as a potential candidate to overcome the environmental pollutants remedy and have been potentially applied for the mineralization of organic pollutants, disinfection of water and air, water-splitting, production of renewable fuels and organic synthesis.[3] Few metal oxides including ZnO, CeO$_2$, WO$_3$, and ZrO$_2$ have also been investigated for the effective removal of industrial pollutants and waste water treatment.[4–7] However, titanium dioxide has been investigated as the best known and most widely used photocatalyst owing to its low cost, less toxicity, high stability, and photocatalytic activity.[8,9] Anatase, rutile, brookite, and TiO$_2$ (B) are the four main crystalline phases of TiO$_2$. Anatase has been investigated much more than other phases of titania due to its intrinsic ability of surface assimilation for organic molecules and low recombination of photogenerated electron–hole pairs.[10] Ordinarily, TiO$_2$ nanoparticles can exhibit excellent photocatalytic efficiency due to efficient charge carrier separation and migration.[11] However, TiO$_2$ nanoparticles (NP) carry several drawbacks as a photocatalyst due to their ultrafine particle size. Moreover, nanoparticles can re-pollute the water because of its difficulty in collecting and recycling the particles from the suspension.[12] TiO$_2$ NP are aggregated so as to minimize their surface area, which degrades their advantages of nanostructure with high surface-to-volume ratios,

making them unsuitable for photocatalysis. On the other hand, one-dimensional (1D) nanostructures have been extensively studied due to their distinctive advantages. Generally, 1D nanostructure had high aspect ratio with the diameter ranging from 1 to 100 nm, and it can be in the rod-, wire-, fiber-, belt–, or tube-shape. Therefore, 1D TiO$_2$ nanostructured materials inherit all the typical features of TiO$_2$ nanoparticles and display a large specific surface area which is easy for the photogenerated charge carriers to transfer along the axial direction. High surface area of the nanofibers has received immense attention due to their unique physical and chemical characteristics, low density, better light absorption, easier charge transport than other nanostructured forms making full use of the benefits of nanostructures in recent years.[13–19] In addition, the ease of their production adds to their advantage than other several techniques, including freeze-drying method, sol–gel method, thermal evaporation, hydrothermal method, and electrospinning. Electrospinning has been recognized as an efficient technique for the fabrication of nanofibers because of its low cost, versatile, simple, and continuous processing.[20–24] This electrostatic processing strategy can be used to fabricate fibrous organic or inorganic mats composed of nano/microscale fibers.

In addition, it has been widely demonstrated that photocatalytic performance depends strongly on the specific surface area, morphology, and crystal phase of TiO$_2$.[13,24,25] Annealing at different temperatures not only influences the morphology but it also controls the crystallinity and structural properties. A relatively low specific surface area on the smooth surface and single crystal phase may pose certain constraints on their performances. Moreover, wide band gap of TiO$_2$ (anatase: 3.2 eV, rutile: 3.0 eV) occupy only 3–5% of the total solar spectrum. Besides this, fast recombination of photogenerated electron–hole pairs also decreases the efficiency in the photocatalytic activity. Thus, the wide application of 1D TiO$_2$ nanostructured materials in some fields was limited due to these critical issues. TiO$_2$ nanofibers owns the following advantages to overcome these problems: (i) High specific surface area especially in case of porous fibers, (ii) controllable pore sizes among the nanofibers ranging from tens to hundreds of nanometers and (iii) the thickness of the fibrous mat, which can be readily tailored. The high specific surface areas of electrospun TiO$_2$ nanofiber mats yields greater number of reaction sites, which consequently enhance the photocatalytic efficiency. Fortunately, 1D TiO$_2$ hetrostructures can be designed and fabricated by introducing another phase with a special morphology (nanorods, nanowires, and nanofibers), to overcome the above mentioned problems. Additionally, it has been reported that the electrospinning process with side by side dual spinnerets could be a simple approach for the fabrication of bi-component TiO$_2$/SnO$_2$ nanofibers with controlled hetrojunctions. Such a structure would lead to an increase in the charge separation of the photogenerated electrons and holes within the bi-component system, allowing both electrons and holes to participate in overall photocatalytic reaction.[26] Based on this assumption, multi-component (anatase and rutile) photocatalystic materials in the form of 1D nanofibers could be more photoactive than a single component photocatalyst owning to their synergistic effect due to the anatase and rutile coexistence.[27]

The catalytic activity takes place at the interface between the catalyst and the reactants only on specific locations of the catalyst's surface, termed as active sites. Therefore, the performance of a catalyst depends on the availability of suitable active sites. Activity is expected to increase with the specific area of the catalyst. However, activity correlations based on this parameter alone are not adequate. The catalyst nature, concentration, and accessibility of the active sites must be considered to find the true activity of a catalyst. It is difficult to count the active sites directly, therefore, for the quantitative measurement of the catalytic activity, turnover frequency (TOF) is a useful assessment for comparing the activity of a catalyst by the active sites. It is simply defined as the number of reactant molecules converted per minute per catalytic site for given reaction conditions.[28]

Our current work focuses on the effect of annealing temperature on the morphology, crystal structure, the phase transformation (from anatase to rutile), band gap and the resultant photocatalytic activity of TiO$_2$ nanofibers. Moreover, TOF was introduced to evaluate the intrinsic photocatalytic activity of TiO$_2$ nanofibers. The aim of this study is to understand that how phase ratios of anatase and rutile affect the photocatalytic activity as well as intrinsic activity. In our work, TiO$_2$ nanofibers with optimal phase ratio of $A/R = 83/17$ have good photocatalytic and intrinsic activities. For comparison, commercially available Degussa P25 was used directly for the photocatalytic and intrinsic activity as a reference.

II. EXPERIMENTAL SECTION

A. Materials and methods

All materials were of analytical grade and used without further purification. Polyvinylpyrrolidone (PVP, $M_w = 1.3 \times 10^6$) was purchased from Aladdin Chemistry Co. Ltd. (Shanghai, China). Tetra-n-butyl titanate (TBT, $\geq$ 98.0%), acetic acid (CH$_3$COOH, $\geq$ 99.5%) and ethanol were purchased from Sinopharm Chemical Reagent Co. Ltd. (Beijing, China). Degussa P25 was purchased from Sigma-Aldrich (St. Louis, Missouri) ($\geq$99.5%).

B. Synthesis of TiO$_2$ nanofibers

For electrospinning of polymeric precursor fibers, 0.9 g of PVP was mixed with 10 mL of ethanol followed by the addition of 3 mL acetic acid and stirred for 2 h.

Subsequently, 1.5 g of TBT was added to this mixture and magnetically stirred at room temperature until the solution became clear and homogeneous. The prepared solution was loaded into a plastic syringe with a stainless steel nozzle (anode) and the tip of the nozzle was placed in the front of a metal cathode with a fixed distance of 15 cm between the nozzle and the collector. An electrical potential of 15 kV was applied for the electrospinning of the fibers at a constant flow rate of 0.5 mL h^{-1}. The resultant dense fibrous mat was collected and dried at 80 °C for 12 h to hydrolyze TBT completely. Afterward, annealing of as-spun TiO_2/PVP nanofibers was carried out at the desired temperatures ranging from 500 to 900 °C for 3 h with the heating rate of 0.5 °C min^{-1}, followed by furnace-cool to ambient temperature. The resulting samples were named as TNF500, TNF600, TNF650, TNF700, TNF750, TNF850, and TNF900 after annealing them at 500, 600, 650, 700, 750, 850, and 900 °C respectively. For comparison, commercially available Degussa P25 was used directly for the photocatalytic activity reference.

C. Characterization

The surface morphologies of TiO_2 nanofibers were examined using the scanning electron microscopy (Hitachi S-4800, Hitachi Corp., Tokyo, Japan) system. X-ray powder diffraction patterns were obtained, using a powder x-ray diffractometer (Rigaku Corporation, Tokyo, Japan, Cu K$_\alpha$ radiation, λ = 1.54178 Å) over Bragg's angles ranging from 10° to 80°. The fraction of anatase-to-rutile transformation in the samples annealed at different temperatures can be calculated from the XRD intensity peaks using the following equation,[29]

$$x = 1/\{1 + 0.8 (I_A/I_R)\} \quad . \quad (1)$$

Where x is the weight fraction of rutile in the nanofibers, I_R is the intensity of rutile peak, and I_A is the intensity of anatase peak. Crystallite sizes for each sample were calculated from the half-height width of the characteristic peaks of anatase (101) and rutile (110) using the Scherrer formula,[30]

$$D = k\lambda/\beta \cos \theta \quad . \quad (2)$$

Where D is the crystallite size, k is the shape constant, λ and θ are the wave length and angle of x-rays. The band gap was determined by UV–Vis diffuse reflectance spectroscopy (DRS) performed at room temperature by UV–Vis spectrometer (Hitachi U-4100, Hitachi Corp.) over the wave length ranging from 300 to 800 nm, using $BaSO_4$ as the reflectance standard for the correction of instrumental background. The Kubelka–Munk function was used to determine the band gap values by transforming the original coordinates (reflectance versus wave length to $(\alpha h\nu)^{1/2}$ versus $h\nu$) in accordance with the theoretical equation,

$$(\alpha h\nu)^{1/2} = A(h\nu - E_{bg}) \quad . \quad (3)$$

Where α is the absorption coefficient of the photocatalyst, A is the proportionality constant, E_{bg} is the energy band gap, and $h\nu$ is the incident photon energy. The extrapolation of the linear portion of $(\alpha h\nu)^{1/2}$ curve versus the photon energy $h\nu$ tangent line crossing point gives a good approximation of the band gap energy of the TiO_2 nanofibers. The PL emission spectra were recorded by fluorescence spectrophotometer (F900, Edinburgh Instruments Ltd., Livingston, United Kingdom). The samples were excited at 320 nm and the emission spectra were scanned between 350 and 600 nm wave length ranges. The decay pattern was determined by using the exponential function in following equation,

$$I(t) = B \exp^{(-t/\tau)} \quad . \quad (4)$$

Where τ is the lifetime and $I(t)$ is the intensity at time t. The specific surface area of the samples were measured by Brunauer–Emmett–Teller (BET; Quantachrome Autosorb-1, Quantachrome Instruments, Boynton Beach, Florida). The samples were degassed at 250 °C for 10 h before the measurements. Comparative characterizations with Degussa P25 were also performed.

D. Photocatalytic activity test

For practical applicability, the photocatalytic activity measurement of the resultant products was evaluated by the photodecomposition of methyl orange (MO) aqueous solution as an organic pollutant under simulated solar light and degradation rates were calculated according to the following equation,

$$\text{Degradation} = C/C_0 \times 100 \quad , \quad (5)$$

where C_0 and C are initial and final concentrations of the MO dye. Typically, 20 mg of the as-prepared photocatalyst was suspended into 20 mL MO solution (20 mg L^{-1}) and placed in a double-walled Pyrex glass reactor under magnetic stirring. All the suspensions were magnetically stirred in dark for 2 h to ensure the establishment of adsorption/desorption equilibrium between the photocatalyst and the MO dye. Then the photodegradation experiment was carried out under ambient conditions, where a metal halogen lamp (HQIBT, 400W/D, OSRAM, Munich, Germany) was used as the light source. A double-walled Pyrex glass reactor was used to maintain a constant temperature with a circulating water system to prevent any evaporation during the experiment. An aliquot (1 mL) of the solution was taken at a certain time interval (30 min) during the

photocatalytic reaction, centrifuged and the supernatant was collected to analyze the UV–visible absorption spectrum measurement (Hitachi U-4100 UV–visible spectrophotometer). The change in MO absorbance of the solution was used to monitor the extent of reaction at given irradiation time intervals. For comparison, P25 was also used as a photocatalyst for the degradation of MO with the same concentration and light conditions. The photodegradation of MO could be considered as a pseudo-first-order reaction[31] and its kinetics might be expressed as follows,

$$C = C_0 e^{-kt} \quad . \tag{6}$$

Where "k" is the degradation rate constant and t is the reaction time. Turnover frequency (TOF), of MO degradation was introduced to describe the intrinsic activity of the TiO₂ nanofiber photocatalyst, which was determined according to the following equation,[32]

$$\text{TOF}\left(h^{-1}\right) = \frac{M_{\text{MO}} \cdot \chi}{M_{\text{TiO}_2} \cdot D \cdot t} \quad . \tag{7}$$

Where M_{MO} and M_{TiO2} is the amount of methyl orange dye and TiO₂ nanofiber catalyst used (in moles), χ is the conversion of MO, t is the reaction time, and D is the dispersion of TiO₂ as a fraction of surface-active TiO₂ catalyst, determined by the following equation,

$$D = \frac{\text{SA}}{\frac{1}{M_{\text{TiO}_2}} \cdot \left(N_A \cdot 4\pi r_{\text{Ti}}^2\right)} \quad . \tag{8}$$

Where SA and M_{TiO2} is the surface area and molecular weight of TiO₂ (79.86 g mol⁻¹) respectively. r_{Ti} is the atomic radius of Ti (0.176 nm), and N_A is Avogadro number (6.02 × 10²³).

III. RESULTS AND DISCUSSIONS

A. Characterization of TiO₂ nanofibers

The SEM images of TiO₂ NFs prepared by the electrospinning technique and P25 are shown in Fig. 1. The as-spun precursor fibers are ranged in the size from few to dozens millimeters in length with average diameter of ~500 nm with smooth surfaces [Fig. 1(a)]. It is observed that annealing of as-spun TiO₂ nanofibers significantly altered the surface morphology, as shown in Figs. 1(b)–1(h). The products are of high yields with well-defined fiber shapes, suggesting that the numerous tiny nanoparticles are assembled uniformly in the fiber matrix. When annealed at lower temperatures from 500 to 650 °C, surface of the nanofibers was porous throughout the bodies. Notably, further annealing of NFs to 900 °C resulted in rougher surface due to the excessive grain growth at high temperature.[33] Meanwhile, the average

diameter of the fibers were almost 150 nm and no significant change was observed with the increase in calcination temperature. As the diameter of the nanofibers mainly depends on the electric field strength, distance between the spinneret and collector, and viscosity and flow rate of the polymer solution.[34] Thus, the diameter of all annealed samples of TiO₂ nanofibers are not much different from each other as all the electrospinning parameters are the same for as-spun TiO₂ nanofibers. The SEM image of TiO₂ nanoparticles (Degussa P25) showed the size of the particle around 20 nm [Fig. 1(i)].

The x-ray diffraction (XRD) patterns of all samples are shown in Fig. 2, which displays the gradual changes in the crystal structure with increase in annealing temperature. As indicated from the XRD patterns, TNF500 obtained pure and crystallized anatase phase of TiO₂. Further increase in annealing temperature leads to crystal growth and enhanced crystallinity as clear from the increased intensity of characteristic peak.[39] The rutile peak was observed to nucleate at the interface of anatase particles. Rutile phase formation starts in the nanofibers above 600 °C, as indicated by the presence of separate sets of peak indexed as rutile TiO₂.[35,36] On further increasing the annealing temperature to 900 °C, the anatase phase disappears and almost pure rutile phase of TiO₂ can be observed for TNF900. These phases are corresponding to standard JCPDS file # 21-1272 for anatase and JCPDS file #21-1276 for rutile. The fractions of anatase-to-rutile transformation in the samples are determined by using Eq. (1). The percentage detail is listed in Table 1. The XRD of Degussa P25 shows mixed anatase and rutile phase with the best A/R ratio as nearly A/R ratio for TNF650.

Generally, the activity of a photocatalyst is determined by the surface area, charge transfer rate to the surface of the catalyst and electron–hole recombination rate. Thus, for the higher photocatalytic activity, smaller crystallite size with higher surface area and number of active sites is more effective which increases the charge carrier transfer rate to the surface of catalyst. In our present work, the increase in crystallite size (from 18 to 40 nm for anatase and 34–47 nm for rutile) is observed when the annealing temperature was raised from 500 to 900 °C which significantly influenced the photocatalytic activity.

The optical properties of the samples were measured by DRS at room temperature, shown in Fig. 3. The band gap of TNF500, TNF600, TNF650, TNF700, TNF750, TNF850, and TNF900 and P25 as calculated by Kubelka–Munk function [Eq. (3)] are 3.16, 3.13, 3.02, 3.00, 3.00, 2.99, 2.99, and 3.05 eV, respectively. This band gap fall might be due to the increasing percentage of rutile with increasing annealing temperature. However, it has been demonstrated that band alignment of ~0.4 eV exists between anatase and rutile TiO₂ with a higher electron affinity for anatase which will cause the effective
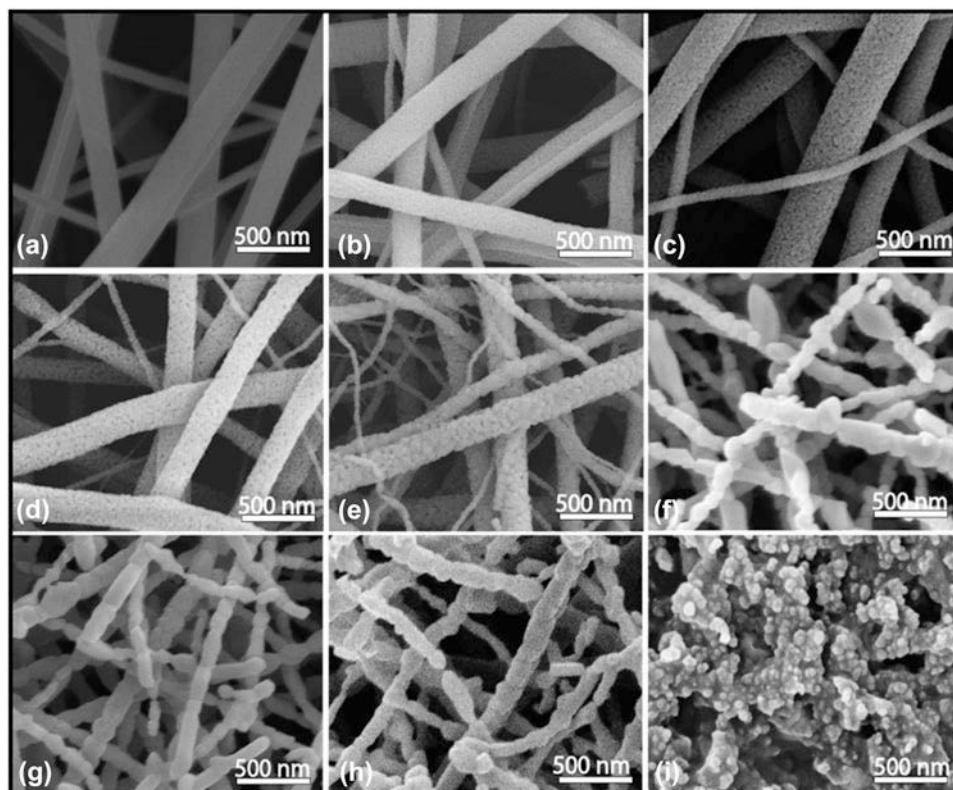
FIG. 1. SEM images of (a) as-spun TNFs (b) TNF500 (c) TNF600 (d) TNF650 (e) TNF700 (f) TNF750 (g) TNF850 (h) TNF900 and (i) P25.
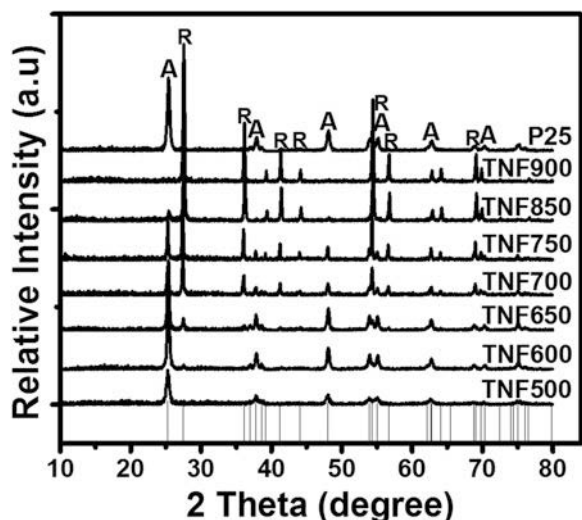

FIG. 2. XRD patterns of TNFs annealed at different temperatures and P25.

TABLE I. The properties of TiO₂ electrospun nanofibers under different heating temperature.

Samples	Average fiber diameter (nm)[a]	Optical band gap (eV)[b]	Crystallite size (nm)[c]		Phase percentage (%)[d]	
			Anatase	Rutile	Anatase	Rutile
P25	...	3.05	20	32	85	15
TNF500	154	3.16	18	...	100	0
TNF600	158	3.13	22	34	93	7
TNF650	159	3.02	25	31	83	17
TNF700	142	3.00	31	32	39	61
TNF750	158	3.00	40	47	30	70
TNF850	161	2.99	37	41	5	95
TNF900	149	2.99	...	44	0	100

[a]Average fiber diameter was directly measured from SEM images of Fig. 1.
[b]Calculated from DRS curves (Fig. 3), using Kubellka-Munk transformation of original coordinates (reflectance versus wave length to $(\alpha h \nu)^{1/2}$ versus $h\nu$) in accordance with the theoretical Eq. (3).
[c]Crystallite sizes were calculated by Scherrer formula [Eq. (2)] based on XRD pattern.
[d]Phase percentage was calculated from XRD intensity peaks using Eq. (1).

separation of photoexcited charge carriers to enhance the photocatalytic activity.[37] In our work, these slight changes in the band gap of TiO₂ nanofibers annealed at different temperatures could be attributed to the synergistic effect of anatase and rutile phases. The band gap of TNF500 was found to be 3.16 eV for the pure anatase phase and band gap of TNF900 was 2.99 eV for the pure rutile. Thus, on increasing the temperature, the incorporation of rutile contents to anatase phase decreased the

band gap from 3.16 to 2.99 eV which is close to the band gap of pure rutile phase (3.0 eV), as listed in Table 1. The effective band gap value of TNF600 (3.13 eV) and TNF650 (3.03 eV) with an optimal ratio for the anatase and rutile phases might be due to the introduction of the rutile phase and approximately the band gap value of

Degussa P25 (3.05 eV). From the absorption spectra between 300 and 800 nm, the optical absorption edge of TiO_2 nanofibers annealed at higher temperatures is shifted to higher wave length as compared to P25 indicating more absorption of light and decreasing band gap with increasing crystallite size, as shown in inset of Fig. 3.

BET surface area analysis was performed to investigate the effect of annealing temperature on the specific surface area, which is one of the prerequisites for the catalytic activity. The measured specific surface areas of the samples P25, TNF500, TNF600, TNF650, TNF700, and TNF900 are 66.2, 43.0, 23.9, 20.1, 11.4, and 6.3 m^2 g^{-1}, respectively, as listed in Table 2. The rest of the samples were skipped for BET because the photocatalytic activity did not show significant differences due to increased percentage of rutile at higher annealing temperatures. As confirmed by XRD, crystallite size increased as annealing temperature increased, resulting in a drop in specific surface area.[38,39]

SEM, XRD, and DRS results (Table 1) reveals that with an increase in annealing temperature, surface becomes rougher due to the crystallite size growth. TNF500 with a band gap value of 3.16 eV, is close to the pure anatase and TNF900 has a band gap value of 2.99 eV close to the pure rutile phase, indicating the transformation of anatase to rutile phase. A fine control of the anatase and rutile ratio and variation in energy gap can be adjusted by annealing temperature and time.[40] Thus, the phase transformation and continuous crystallite size growth with higher annealing temperatures are also confirmed by XRD data. Increasing rutile content should decrease the surface area because anatase to rutile phase transformation takes place at higher temperatures usually greater than 600 °C which is accompanied by excessive grain growth and the surface becomes rougher.[33]
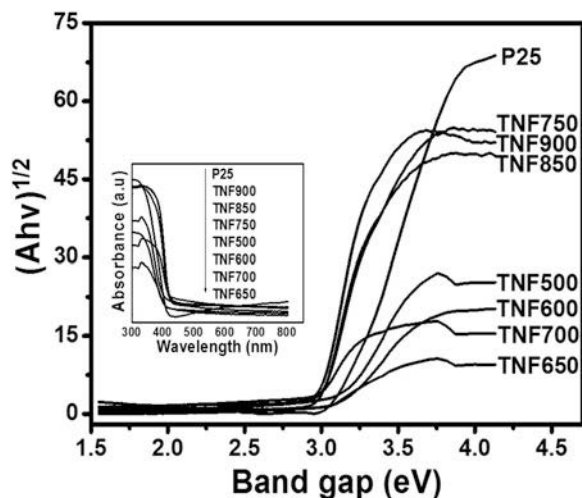
B. Photocatalytic degradation of methyl orange

The photodegradation rate of methyl orange (MO) used to simulate the reaction was investigated to explore the photocatalytic activity of the TiO_2 nanofibers by using Eq. (5), shown in Fig. 4. It can be observed that photocatalytic activity of TiO_2 nanofibers is improved when the annealing temperature of the as-prepared composite nanofibers was increased from 500 to 650 °C. In case of nanofibers annealing at 600 and 650 °C, MO was almost completely degraded within 120 min of illumination. However, annealing beyond 650 °C for the as-prepared nanofibers leads to the deterioration in the photocatalytic activity due to the larger crystallite size at higher temperatures. The degradation rates of MO for TNF500, TNF600, TNF650, TNF700, TNF750, TNF850, and TNF900 are 71, 100, 98, 48, 5, 8, and 3%, respectively. TNF600 and TNF650 exhibited excellent photocatalytic activity among all the tested samples like P25 and the data coordinates well with the exponential function as shown in Fig. 4. These results were in consistent with the previously reported work.[41,42] The

TABLE II. Photocatalytic behavior of TiO₂ nanofibers.

Samples	BET area (m²/g)	Degradation (%)[a]	TOF (h⁻¹)[b]
P25	66.2	55	1175
TNF500	43.0	19	626
TNF600	23.9	39	2309
TNF650	20.1	34	2394
TNF700	11.4	16	1986
TNF900	6.3	1	224

[a]Degradation of MO solution under UV light at 0.5 h of the reaction.
[b]TOF at 0.5 h, the number of reactant molecules that react per site per unit time, was calculated by using Eq. (7).

FIG. 3. UV–Vis-diffuse reflectance spectra of TNFs annealed at different temperatures. Inset shows absorption spectra from 300 to 800 nm.
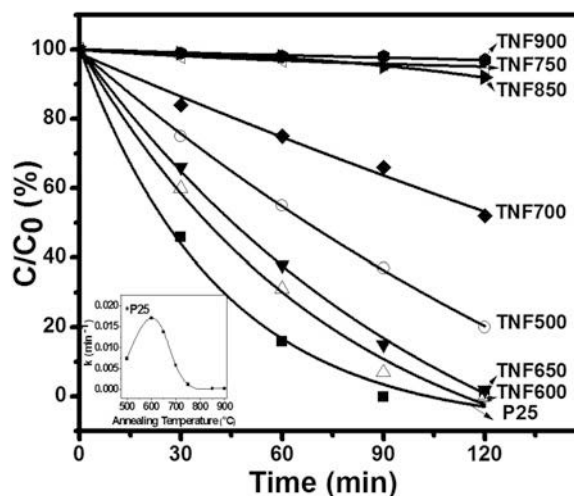

FIG. 4. Photocatalytic performance of MO solution with time in the presence of TNFs annealed at different temperatures and P25 under UV light. Inset is the relationship between the degradation rate constant and annealing temperature.

photodegradation of MO could be considered as a pseudo-first-order reaction and its kinetics might be calculated by Eq. (6). The relationship between degradation rate constant "k" and annealing temperature "T" is shown in the inset of Fig. 4. It shows the highest photocatalytic activity with highest rate constant (k) of 0.0170 min^{-1} where the optimal crystal phase ratio is obtained at 600 °C for the degradation of the MO dye. The best photocatalytic efficiency of TNF600 and TNF650 might be attributed to the optimal phase ratio between the anatase and rutile phases of TiO$_2$ and efficient electron–hole separation due to the good crystallite structure. Electrons appear to have transferred from anatase to rutile trapping sites, which obstruct the charge recombination.[43]

1. Intrinsic photocatalytic activity

The true intrinsic photocatalytic activity for all the samples is calculated by turnover frequency (TOF) using Eq. (7), as listed in Table 2. The maximum TOF value was observed for TNF650 (2394 h^{-1}) after 0.5 h of the MO degradation reaction, almost two times of P25 (1175 h^{-1}). However, BET surface area of the sample TNF650 is lower than P25 but its higher TOF value might be attributed to the presence of a large number of active surface sites for the degradation of methyl orange dye. Higher TOF values of TNFs may be attributed to their higher stability and higher reaction rates than Degussa P25.[44,45] Appropriate crystalline structure with suitable anatase/rutile phase ratio could be the reason for enhanced intrinsic photocatalytic activity of TiO$_2$ nanofibers. PL spectra also provides an evidence for higher TOF of TNF650.

The PL spectra of TNF650 and commercial P25 are shown in Fig. 5. Since, the efficiency of charge carrier trapping, migration, and transfer could greatly affect the

photocatalytic activity. The PL emission intensity is the result of recombination of photo-excited electrons and holes, thus lower PL intensity indicates a lower electron–hole recombination rate. The intensity of TNF650 is slightly lower than P25. It might be ascribed to the lower recombination rate of photoexcited e$^-$–h$^+$ pair which is due to the efficient electron–hole transfer to the fiber's surface. Decay time of TNF650 and P25 (inset of Fig. 5) also provides another evidence of lower electron–hole recombination rate which is well traced using the exponential function of Eq. (4), having a lifetime of 112 μs suggests the existence of carrier trapping sites which leads to the distribution of carrier transport rate.

IV. CONCLUSIONS

In summary, TiO$_2$ nanofibers were fabricated using electrospinning technique followed by annealing at different temperatures. The TiO$_2$ anatase/rutile phase ratio of the fibers was successfully controlled by different annealing temperatures ranging from 500 to 900 °C. The photocatalytic activity of obtained TiO$_2$ nanofibers was evaluated by the decomposition of methyl orange under UV irradiation which shows a strong dependence on the annealing temperature. The optimal annealing temperature is 650 °C, which corresponds to anatase/rutile phase ratio of 83/17, resulting in the best photocatalytic performance closely proportional to P25. This might be attributed to the effective electron–hole separation due to the introduction of mixed anatase-rutile phase. TNF650 acquired the highest TOF value 2394 h^{-1}, two times of P25 with similar anatase/rutile phase ratio (A/R = 85/15). The current work may provide a possible strategy to the future research initiatives for nanofiber photocatalysis based on titanium dioxide.

REFERENCES

1. A. Fujishima and K. Honda: Electrochemical photolysis of water at a semiconductor electrode. *Nature* **238**(5358), 37 (1972).
2. A. Fujishima, T.N. Rao, and D.A. Tryk: Titanium dioxide photocatalysis. *J. Photochem. Photobiol., C* **1**(1), 1 (2000).
3. R. Michael, S.T.M. Hoffmann, W. Choi, and D.W.B. Mannt: Environmental applications of semiconductor photo-catalysis. *Chem. Rev.* **95**(1), 69 (1995).
4. X. Duan, G. Wang, H. Wang, Y. Wang, C. Shen, and W. Cai: Orientable pore-size-distribution of ZnO nanostructures and their superior photocatalytic activity. *CrystEngComm* **12**(10), 2821 (2010).
5. P. Ji, J. Zhang, F. Chen, and M. Anpo: Study of adsorption and degradation of acid orange 7 on the surface of CeO$_2$ under visible light irradiation. *Appl. Catal., B* **85**(3–4), 148 (2009).
6. K. Sayama, H. Hayashi, T. Arai, M. Yanagida, T. Gunji, and H. Sugihara: Highly active WO$_3$ semiconductor photocatalyst prepared
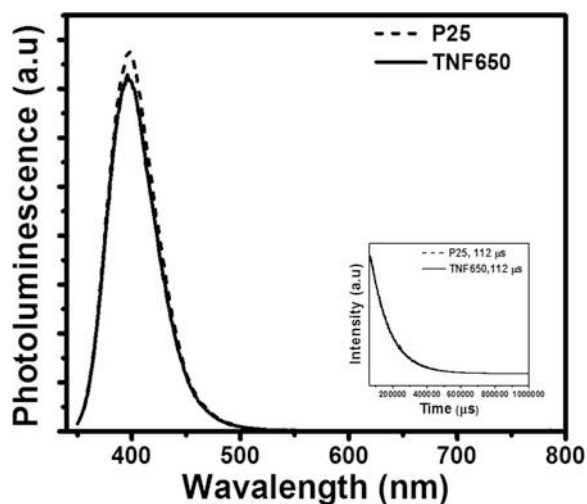

FIG. 5. PL emission peaks for TNF650 and P25. Inset is PL decay curves of TNF650 and P25.

3042

J. Mater. Res., Vol. 31, No. 19, Oct 14, 2016

from amorphous peroxo-tungstic acid for the degradation of various organic compounds. *Appl. Catal., B* **94**(1–2), 150 (2010).

7. V.R. Reddy, D.W. Hwang, and J.S. Lee: Photocatalytic water splitting over ZrO$_2$ prepared by precipitation method. *Korean J. Chem. Eng.* **20**(6), 1026 (2003).

8. W. Bahnemann, M. Muneer, and M.M. Haque: Titanium dioxide-mediated photocatalysed degradation of few selected organic pollutants in aqueous suspensions. *Catal. Today* **124**(3–4), 133 (2007).

9. K. Nakata and A. Fujishima: TiO$_2$ photocatalysis: Design and applications. *J. Photochem. Photobiol., C* **13**(3), 169 (2012).

10. L. Liu, H. Zhao, J.M. Andino, and Y. Li: Photocatalytic CO$_2$ reduction with H$_2$O on TiO$_2$ nanocrystals: Comparison of anatase, rutile and brookite polymorphs and exploration of surface chemistry. *ACS Catal.* **2**(8), 1817 (2012).

11. M.A. Fox and M.T. Dulay: Hetrogeneous photocatalysis. *Chem. Rev.* **93**(1), 341 (1993).

12. J.R. Jennings, A. Ghicov, L.M. Peter, P. Schmuki, and A.B. Walker: Dye-sensitized solar cells based on oriented TiO$_2$ nanotube arrays: Transport, trapping and transfer of electrons. *J. Am. Chem. Soc.* **130**(40), 13364 (2008).

13. L. Mai, X. Tian, X. Xu, L. Chang, and L. Xu: Nanowire electrodes for electrochemical energy storage devices. *Chem. Rev.* **114**(23), 11828 (2014).

14. Z. Zheng, Y. Cheng, X. Yan, R. Wang, and P. Zhang: Enhanced electrochemical properties of graphene-wrapped ZnMn$_2$O$_4$ nanorods for lithium-ion batteries. *J. Mater. Chem. A* **2**(1), 149 (2014).

15. V. Aravindan, J. Sundaramurthy, P.S. Kumar, Y.S. Lee, S. Ramakrishna, and S. Madhavi: Electrospun nanofibers: A perspective electro-active material for constructing high performance Li-ion batteries. *Chem. Commun.* **51**(12), 2225 (2015).

16. Y.N. Xia, P.D. Yang, Y.G. Sun, Y.Y. Wu, B. Mayers, B. Gates, Y.D. Yin, F. Kim, and Y.Q. Yan: One-dimensional nanostructures: Synthesis, characterization and applications. *Adv. Mater.* **15**(5), 353 (2003).

17. J. Wang, G. Yang, L. Wang, and W. Yan: Fabrication of a well-aligned TiO$_2$ nanofiberous membrane by modified parallel electrode configuration with enhanced photocatalytic performance. *RSC Adv.* **6**(37), 31476 (2016).

18. D. Li and Y. Xia: Fabrication of titania nanofibers by electrospinning. *Nano Lett.* **3**(4), 555 (2003).

19. W. Nuansing, S. Ninmuang, W. Jarernboon, S. Maensiri, and S. Seraphin: Structural characterization and morphology of electrospun TiO$_2$ nanofibers. *Mater. Sci. Eng., B* **131**(1–3), 147 (2006).

20. M. Ge, C. Cao, J. Huang, S. Li, Z. Chen, K.Q. Zhang, S.S. Al-Deyab, and Y. Lai: A review of one-dimensional TiO$_2$ nanostructured materials for environmental and energy applications. *J. Mater. Chem. A* **4**(18), 6772 (2016).

21. J.W. Jung, C.L. Lee, S. Yu, and I.D. Kim: Electrospun nanofibers as a platform for advanced secondary batteries: A comprehensive review. *J. Mater. Chem. A* **4**(3), 703–750 (2016).

22. X. Chen and S.S. Mao: Titanium dioxide nanomaterials: Synthesis, properties, modifications and applications. *Chem. Rev.* **107**(7), 2891 (2007).

23. P.S. Kumar, J. Sundaramurthy, S. Sundarrajan, V.J. Babu, G. Singh, S.I. Allakhverdiev, and S. Ramakrishna: Hierarchical electrospun nanofibers for energy harvesting production and environmental remediation. *Energy Environ. Sci.* **7**(10), 3192 (2014).

24. C. Tealdi, E. Quartarone, P. Galinetto, M.S. Grandi, and P. Mustarelli: Flexible deposition of TiO$_2$ electrodes for photocatalytic applications: Modulation of the crystal phase as a function of the layer thickness. *J. Solid State Chem.* **199**, 1 (2013).

25. W. Sun, H. Liu, J. Hu, and J. Li: Controllable synthesis and morphology-dependent photocatalytic performance of anatase TiO$_2$ nanoplates. *RSC Adv.* **5**(1), 513 (2015).

26. H. Hou, L. Wang, F. Gao, G. Wei, J. Zheng, B. Tang, and W. Yang: Hierarchically porous TiO$_2$/SiO$_2$ fibers with enhanced photocatalytic activity. *RSC Adv.* **4**(38), 19939 (2014).

27. D. Ma, L.S. Schadler, R.W. Siegel, and J. Hong: Preparation and structure investigation of nanoparticle-assembled titanium dioxide microtubes. *Appl. Phys. Lett.* **83**(9), 1839 (2003).

28. Y. Lei, L.D. Zhang, G.W. Meng, G.H. Li, X.Y. Zhang, C.H. Liang, W. Chen, and S.X. Wang: Preparation and photoluminescence of highly ordered TiO$_2$ nanowires arrays. *Appl. Phys. Lett.* **78**(8), 1125 (2001).

29. R.A. Spurr and H. Myers: Quantitative analysis of anatase-rutile mixtures with an x-ray diffractometer. *Anal. Chem.* **29**(6), 760 (1957).

30. B.D. Cullity: *Elements of X-ray Diffraction* (Addison–Wesley, Reading, MA, 1978).

31. Q. Wan, T.H. Wang, and J.C. Zhao: Enhanced photocatalytic activity of ZnO nanotetrapods. *Appl. Phys. Lett.* **87**(8), 083105 (2005).

32. C. Zhou, Y. Chen, Z. Guo, X. Wang, and Y. Yang: Promoted aerobic oxidation of benzyl alcohol on CNT supported platinum by iron oxide. *Chem. Commun.* **47**(26), 7473 (2011).

33. S. Bakardjieva, J. Subrt, V. Stengl, M.J. Dianez, and M. Sayagues: Photoactivity of anatase-rutile TiO$_2$ nanocrystalline mixtures obtained by heat treatment of homogeneously precipitated anatase. *Appl. Catal., B* **58**(3–4), 193 (2005).

34. Z.M. Huang, Y.Z. Zhang, M. Kotaki, and S. Ramakrishna: A review on polymer nanofibers by electrospinning and their applications in nanocomposites. *Compos. Sci. Technol.* **63**(15), 2223 (2003).

35. L.H. Edelson and A.M. Glaeser: Role of particle substructure in the sintering of monosized titania. *J. Am. Ceram. Soc.* **71**(4), 225 (1988).

36. H. Zhang and J.F. Banfield: Phase transformation of nanocrystalline anatase-to-rutile via combined interface and surface nucleation. *J. Mater. Res.* **15**(2), 437–448 (2000).

37. N.T. Nolan, M.K. Seery, S.J. Hinder, L.F. Healy, and S.C. Pillai: A systematic study of the effect of silver on the chelation of formic acid to a titanium precursor and the resulting effect on the anatase to rutile transformation of TiO$_2$. *J. Phys. Chem. C* **114**(30), 13026 (2010).

38. D.O. Scanlon, C.W. Dunnill, J. Buckeridge, S.A. Shevlin, A.J. Logsdail, S.M. Woodley, C.R.A. Catlow, M.J. Powell, R.G. Palgrave, I.P. Parkin, G.W. Watson, T.W. Keal, P. Sherwood, A. Walsh, and A.A. Sokol: Band alignment of rutile and anatse TiO$_2$. *Nat. Mater.* **12**(9), 798–801 (2013).

39. D. Vu, X. Li, Z. Li, and C. Wang: Phase-structure effects of electrospun TiO$_2$ nanofiber membrane on As(III) adsorption. *J. Chem. Eng. Data* **58**(1), 71 (2013).

40. H. Li, W. Zhang, B. Li, and W. Pan: Diameter dependent photocatalytic activity of electrospun TiO$_2$ nanofiber. *J. Am. Ceram. Soc.* **93**(9), 2503 (2010).

41. E. Kordouli, V. Dracopoulos, T. Vaimakis, K. Bourikas, A. Lycourghiotis, and C. Kordulis: Comparative study of phase transition and textural changes upon calcination of two commercial titania samples: A pure anatase and a mixed anatase-rutile. *J. Solid State Chem.* **232**, 42 (2015).

42. H. Li, W. Zhang, and W. Pan: Enhanced photocatalytic activity of electrospun TiO$_2$ nanofibers with optimal anatase/rutile ratio. *J. Am. Ceram. Soc.* **94**(10), 3184 (2011).

43. C.C. Pei and W.W.F. Leung: Enhanced photocatalytic activity of electrospun TiO$_2$/ZnO nanofibers with optimal anatase/rutile ratio. *Catal. Commun.* **37**, 100 (2013).

44. G. Li and K.A. Gray: The solid–solid interface: Explaining the high and unique photocatalytic reactivity of TiO$_2$-based nanocomposite materials. *Chem. Phys.* **339**(1–3), 173 (2007).

45. M. Boudart: Turnover rates in heterogeneous catalysis. *Chem. Rev.* **95**(3), 661 (1995).